

PACS numbers: 42.55.Tv; 42.55.Px; 73.61.Ey
DOI: 10.1070/QE2013v043n11ABEH015127

Optimisation of optical properties of a long-wavelength GaInNAs quantum-well laser diode

M.S. Alias, A.N. Al-Omari, F. Maskuriy, F. Faiz, S.M. Mitani

Abstract. **We report optimisation of optical properties of a strained GaInNAs/GaAs quantum-well laser, by taking into account the many-body effect theory and the bowing parameter. The theoretical transition energies and the GaInNAs bowing parameter are fitted into the photoluminescence spectrum of the GaInNAs quantum well, obtained in the experiment. The theoretical results for the photoluminescence spectrum and laser characteristics (light, current and voltage) exhibits a high degree of agreement with the experimental results.**

Keywords: *GaInNAs, edge emitting laser, laser diode.*

1. Introduction

Long-wavelength laser diodes, especially those emitting at 1.3 μm, now attract researchers' interest because this wavelength is widely used as an upstream transmission wavelength in such optical fibre access networks as fibre-to-the-home (FTTH), radio-over-fibre (RoF) and optical interconnections. Conventionally, long-wavelength laser diodes are grown on InP-based materials such as InGaAsP/InP quantum wells (QWs). However, the InGaAsP/InP QW laser requires thermal cooling due to its low characteristic temperature (around 60 K) [1], which leads to the use of more expensive components for optical network systems. The low characteristic temperature of such lasers is caused by poor confinement of electrons in the conduction band due to its marginal conduction band offset ($\Delta E_c = 0.4\,\Delta E_g$) [2]. In comparison, a GaAs-based laser diode exhibits a higher characteristic temperature; however, it is typically used at shorter wavelengths (0.85 to 1 μm). In order to overcome the InGaAsP/InP QW material limitation, the GaAs-based long-wavelength laser diode research has been pursued in recent years by developing new material systems such as highly strained InGaAs/GaAs QWs, InAs/GaAs quantum dots (QDs), GaInNAs/GaAs and GaInNAsSb/GaAs QWs [3]. In the GaInNAs/GaAs QW material, for example, the presence of a substantial conduction band ($\Delta E_c = 0.79\,\Delta E_g$) has been demonstrated [4], resulting in a significant confinement of electrons and in an increase in the GaInNAs laser diode characteristic temperature up to 138 K [5]. As a result, an uncooled laser diode can be realised in an effort to reduce the low-cost and thermally stable optical network component.

In this paper, in reference to actual laser devices fabricated, we study theoretically the optimised optical properties of a GaInNAs/GaAs QW laser, taking into account the many-body effect theory and the fitted bowing parameter. To the best of our knowledge, only several papers dealing with the theoretical studies on GaInNAs laser diodes have been published so far. However, these papers are mainly devoted to the VCSEL technology [6, 7] rather than to the edge-emitting laser (EEL) proposed here.

2. Experiment and device model

2.1. Device structure and fabrication

The GaInNAs samples under study are grown by the molecular beam epitaxy (MBE) in the Riber 32P reactor using Ga, As and In solid sources, and an N radio-frequency plasma source. After growth, the samples are annealed at 700 °C for 80 min under As overpressure. According to the photoluminescence (PL) data, the sample consists of a $Ga_{0.66}In_{0.34}N_{0.014}As_{0.986}$ QW with the thickness $d_{QW} = 7$ nm embedded between GaAs barriers with the thickness of 85 nm and 170 nm for top- and bottom-barriers, respectively. All layers are undoped and grown on a n-GaAs substrate (001) (Fig. 1).

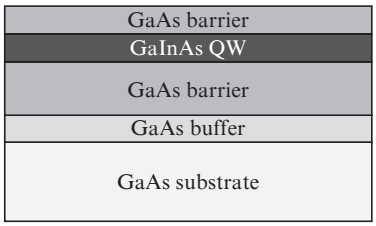

Figure 1. Schematic cross section of the GaInNAs QW sample.

The laser diode consists of an intentionally undoped 8.8-nm-thick $Ga_{0.65}In_{0.35}N_{0.01}As_{0.99}$ QW embedded between GaAs barriers with the thickness of 150 nm each. The top and bottom spacers are formed by 200-nm-thick undoped $Al_{0.35}Ga_{0.65}As$. The n-cladding layer consists of 1.3-μm-thick $Al_{0.35}Ga_{0.65}As$ doped with Si at a concentration from 3.4 to 1×10^{18} cm^{-3} (bottom to top). The p-cladding layer is formed by 1.3-μm-thick $Al_{0.35}Ga_{0.65}As$ heavily doped with beryllium at a concentration from 1 to 3.4×10^{18} cm^{-3} (bottom to top). The epiwafer is capped with a 150-nm-thick GaAs cap layer heavily doped with beryllium (1×10^{19} cm^{-3}) (Fig. 2). The

M.S. Alias, F. Maskuriy, F. Faiz, S.M. Mitani Advanced Physical Technologies Laboratory, Telekom Malaysia Research & Development, Lingkaran Teknokrat Timur, 63000 Cyberjaya, Selangor, Malaysia; e-mail: drsharizal@gmail.com;
A.N. Al-Omari Electronic Engineering Department, Hijjawi Faculty for Engineering Technology, Yarmouk University, Irbid 21163, Jordan

Received 22 January 2013
Kvantovaya Elektronika **43** (11) 1009–1013 (2013)
Submitted in English

GaInNAs laser diode fabrication started with the thinning of the substrate followed by metallisation of the bottom n- and the top p-ohmic contacts by sputtering AuGe/Au and Au/AuZn/Au, respectively. The bottom n-contact was formed by straightforward deposition; however, the top p-contact required photolithography patterning, wet chemical etching, passivation and lift-off. After these processing steps were completed, the device was cleaved to form the mirror facets. The measurements were performed at room temperature under pulsed operation (a pulse duration of 1 μs and a duty cycle of 0.1 %). The light– current (L–I) and current–voltage (I–V) characteristics were measured by varying precisely the input current (using a semiconductor parameter analyser). The light output was detected with a Ge photodetector which was also connected to the semiconductor parameter analyser. The output spectrum of the EEL was measured by coupling the lasing beam into an optical fibre connected to the optical spectrum analyser. The PL was observed at 17 K using a 514.5-nm line of the Ar laser and a liquid nitrogen cooled Ge detector.

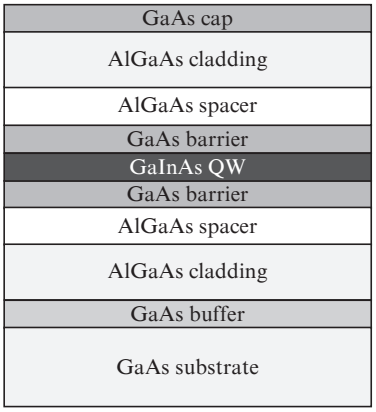

Figure 2. Schematic cross section of the GaInNAs laser diode structure.

2.2. Device model

The numerical simulation is performed using a Photonics Integrated Circuit Simulator in 3D (PICS3D), which is a physically based self-consistent semiconductor laser simulator. The optical gain of the GaInNAs QW is computed using the Coulomb enhanced gain spectral function as below [8] in order to include the many-body effect into the laser model:

$$g(\hbar\omega) = \mathrm{Re}\left\{\int_{E_{g0}}^{\infty} \frac{g_0(E_{cv})}{1-q_1(E_{cv},\hbar\omega)}\left[1 - \mathrm{i}\frac{E_{cv}-\hbar\omega}{\Gamma_{cv}}\right] \times L(\hbar\omega - E_{cv})\,\mathrm{d}E_{cv}\right\}, \quad (1)$$

where

$$q_1(E_{cv},\hbar\omega) = -\mathrm{i}\frac{a_0 E_0 E_{cv}}{\pi\kappa|M_{ji}(E_{cv})|}\int_0^{\infty}\mathrm{d}k'\,k'\frac{|M_{ji}(E_{cv'})|}{E_{cv'}} \times \frac{f_e(E_{cjk'}) + f_h(E_{vjk'}) - 1}{\Gamma_{cv} + \mathrm{i}(E_{cv} - \hbar\omega)}\Theta(k,k'); \quad (2)$$

$$\Theta(k,k') = \int_0^{2\pi}\frac{1 + C_{pl}\kappa a_0 q^2 (32\pi N_{2D})^{-1}}{1 + q/\kappa + C_{pl}\kappa a_0 q k'^3 (32\pi N_{2D})^{-1}}\mathrm{d}\theta; \quad (3)$$

$$q^2 = k^2 + k'^2 - 2kk'\cos\theta; \quad (4)$$

θ is the angle between in-plane vectors k and k'; the factor $1(1 - q_1)^{-1}$ represents the Coulomb enhancement in the Pade approximation [8, 9]; $a_0 = 4\pi\hbar^2\varepsilon_b\varepsilon_0/(e^2 m_{rj})$ is the exciton Bohr radius; $E_0 = \hbar^2/(2m_{rj}a_0^2)$ is the corresponding Rydberg energy; $E_{cv}(k) = E_g + \Delta E_g + E_{cjk} + E_{vik}$; C_{pl} is the dimensionless constant typically in a range 1 to 4; κ is the inverse screening length for electrons and holes confined in the quantum well; ε_b is the static background dielectric constant in the area of the quantum well; and $N_{2D} = n_e d_{QW}$ is the two-dimensional carrier density in the QW.

In obtaining material parameters for the $Ga_xIn_{1-x}N_{1-y}As_y$ material system, a linear interpolation between the parameters of the relevant binary semiconductors is calculated except for the energy bandgap. The physical parameter P of the interpolation expression is given as

$$P_{GaInNAs} = xyP_{GaAs} + x(1-y)P_{GaN} + (1-x)yP_{InAs} + (1-x)(1-y)P_{InN}, \quad (5)$$

where x and y are the Ga and As contents, respectively. Considering the bandgap bowing of GaNAs and InGaAs, the temperature dependent energy bandgap of GaInNAs is expressed as [10]:

$$E_{g\,GaInNAs} = xyE_{g\,GaAs} + x(1-y)E_{g\,GaN} + (1-x)yE_{g\,InAs} + (1-x)(1-y)E_{g\,InN} + xy(1-y)b_{GaNAs} + xy(1-x)b_{InGaAs} - 5.5\times10^{-4}\left[\frac{T^2}{T+225} - \frac{300^2}{300+225}\right], \quad (6)$$

where b_{GaNAs} and b_{InGaAs} are the bowing parameters of GaNAs and InGaAs, and T is the absolute temperature.

The material parameters of the binary semiconductors used in this study such as the Luttinger parameters, elastic stiffness constants, hydrostatic deformation potential, shear deformation potential, effective masses of electrons and holes and lattice constant are listed in Table 1.

3. Results and discussion

Figure 3 shows the calculated PL spectrum for the GaInNAs QW at various bowing parameters of GaAsN (from –16.5 to

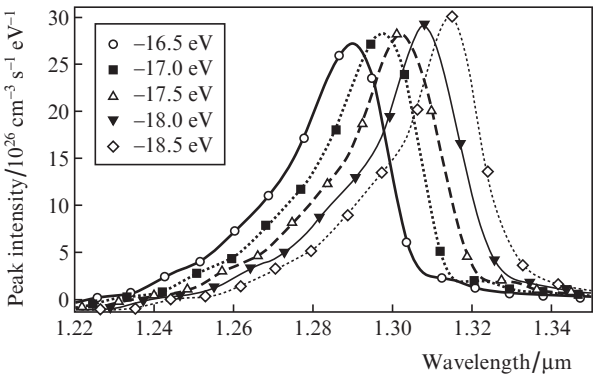

Figure 3. Calculated PL spectra of the GaInNAs QW at different values of the b_{GaNAs} parameter.

Table 1. Material parameters of binary semiconductors.

Parameter	GaAs	InAs	GaN	InN
Lattice constant a_0/Å	5.65325	6.0584	4.5	4.98
Hydrostatic deformation potential for conduction band a_c/eV	–9.77	–6.0	–7.4	–3.35
Hydrostatic deformation potential for valence band a_v/eV	1.16	1.00	–	–
Shear deformation potential b/eV	–1.7	–1.8	–2.2	–1.2
Elastic stiffness constants: $C_{11}/10^{11}$ dyn cm^{-2}	11.9	8.33	2.93	1.87
$C_{12}/10^{11}$ dyn cm^{-2}	5.38	4.53	1.59	1.25
Luttinger parameters: γ_1	6.85	20.4	2.67	3.72
γ_2	2.1	8.3	0.75	1.26
γ_3	2.9	9.1	1.10	1.63
Electron effective mass m_e/m_0	0.064	0.023	0.15	0.12
Heavy-hole effective mass m_{hh}/m_0	0.50	0.40	0.80	0.80
Light-hole effective mass m_{lh}/m_0	0.091	0.208	0.21	0.19
Spin-orbit split-off energy Δ/V	0.34	0.43	0.017	0.006
Energy bandgap E_g/eV	1.424	0.417	3.299	0.735

–18.5 eV) and at a constant InGaAs bowing parameter (–4.77 eV) [11]. As the value of b_{GaAsN} increases, the peak intensity of the PL increases from 2.6×10^{27} to 3.0×10^{27} cm^{-3} s^{-1} eV^{-1} and the spectrum maximum is red-shifted from 1.285 to 1.315 μm, respectively. In addition, the full-width at half-maximum (FWHM) of the PL spectrum decreases from approximately 29 nm to 23 nm as the GaAsN bowing parameter increases. The PL broadening is due to nitrogen incorporation which degrades the GaInNAs QW crystallinity where nitrogen could out-diffuse and create phase segregations during the crystal growth.

Figure 4 exhibits the theoretical results of the GaInNAs QW material gain at different GaNAs bowing parameters as a function of wavelength with the carrier density injection of 1.5×10^{18} cm^{-3}. The operation wavelength of interest (1.3 μm) is achieved when b_{GaNAs} is around –17.0 to –17.5 eV. Although the GaNAs bowing parameter is varied, the peak of the material gain of the GaInNAs QW is approximately the same (around 2500 cm^{-1}) for all b_{GaNAs} values from –16.5 to –18.5 eV (Fig. 4). This is verified by computing the peak of the material gain for various GaNAs bowing parameters as a function of the carrier density injection for the GaInNAs QW (Fig. 5). It can be seen that the behaviour of the material gain peaks for all GaNAs bowing parameters is similar for a given carrier density injection value since the composition of the GaInNAs QW is the same (66% Ga, 34% In, 1.4% N and 98.6% As).

In order to analytically determine the exact GaNAs bowing parameter for the grown GaInNAs QW with the composition

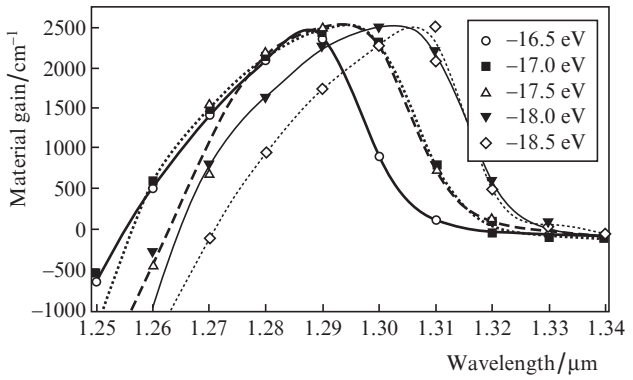

Figure 4. Material gain spectra of the GaInNAs QW at different values of the b_{GaNAs} parameter.

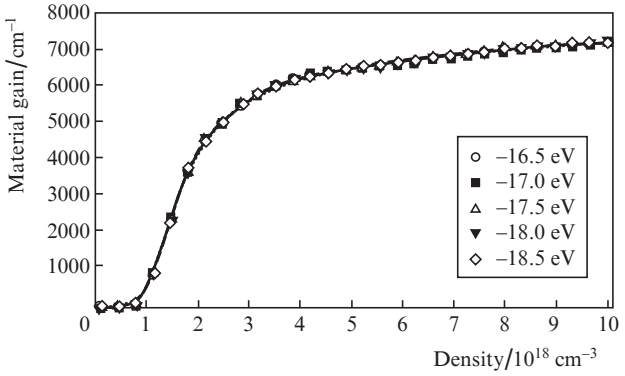

Figure 5. Peak material gain as a function of carrier density injection for the GaInNAs QW at different values of the b_{GaNAs} parameter.

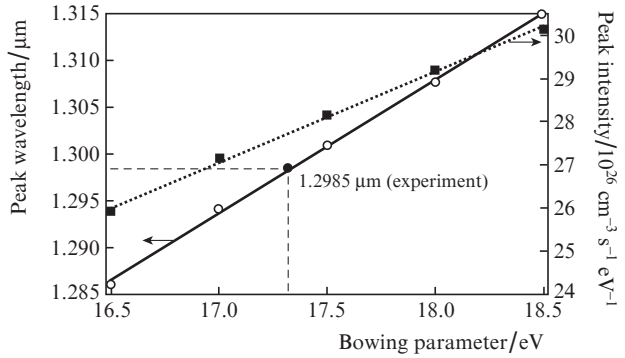

Figure 6. Peak wavelength and peak intensity as a function of the GaNAs bowing parameter.

mentioned above, the peak wavelength and peak intensity from the computed PL spectrum is plotted as functions of b_{GaNAs} (Fig. 6). From the experimental PL measurements, the grown GaInNAs QW emission wavelength is around 1.285 μm, and when this value is plotted in the same graph the results indicate that the GaNAs bowing parameter is approximately –17.3 eV. The obtained value is within the range of the reported GaNAs bowing parameter which is from –16.9 to 25 eV [11, 12] depending on the GaInNAs material composition.

The obtained theoretical values of GaNAs and InGaAs bowing parameters are then incorporated into the PL spectrum computation using the actual PL sample structure. Figure 7 shows the comparison between the computed PL spectrum

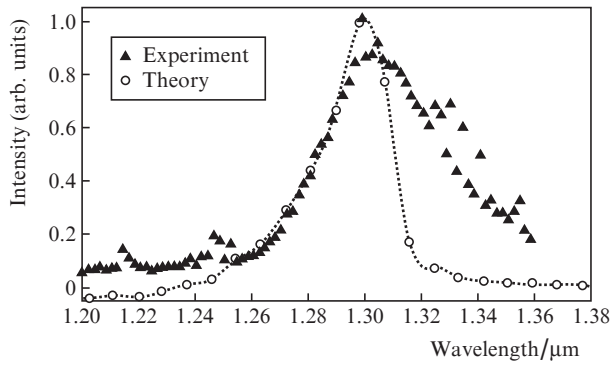

Figure 7. Theoretical and experimental PL spectra of the GaInNAs QW.

and the measured PL spectrum from the grown GaInNAs QW sample. The result indicates a high degree of agreement between theoretical and experimental PL spectra. The GaInNAs QW emits at the equivalent wavelength which is 1.285 μm. However, the PL broadening is different: the FWHM of the measured PL spectrum is much broader than that of the computed PL spectrum. This result is somewhat expected because the theoretical study does not take into account the effect of the growth quality which is one of the difficulty in growing the GaInNAs material either by the MBE or metal-organic chemical vapour deposition (MOCVD) technique. Nevertheless, the PL spectra demonstrate a similar behaviour in the region of shorter wavelengths. At longer wavelengths, the discrepancy evolves since the increase in the nitrogen content in the GaInNAs material system will deteriorate the growth quality due to a small atomic radius and a high electronegativity of nitrogen atoms [13].

Once the optical characteristics of the GaInNAs QW are optimised and the computed analysis is fitted to actual experimental measurements, we performed an analysis of the fabricated GaInNAs laser diode. Figure 8 shows the light–current (L–I) characteristic for the simulated and fabricated GaInNAs laser diodes with a stripe width of 50 μm and a cavity length of 740 μm. The fitted GaInNAs theoretical device model illustrated a very good L–I characteristic agreement with the fabricated device. At a temperature of 300 K, the threshold current obtained was around 0.33 A. Based on the GaInNAs laser diode active region geometry, the threshold current density was around 0.88 kA cm^{-2}. The low values achieved for the threshold current and the threshold carrier density indicate the excellent quality of the designed and grown GaInNAs QW.

Figure 9 shows the calculated and experimental current–voltage (I–V) characteristic of the GaInNAs laser diode. The turn-on voltage is approximately 0.97 V, corresponding to the bandgap of the GaInNAs QW at 1.285 μm. The slope of the I–V curve which is determined by the device series resistance is around 2.82 Ω. This value is lower than the device series resistance for the fabricated device, which is around 3.67 Ω. The difference is due to the effect of the actual growth quality of the fabricated device (where probable defects emerged in growing the GaInNAs QW material) and fabrication of device metallisation contacts. Although the simulated device and fabricated device series resistances deviate marginally, a good agreement between theoretical and experimental results is obtained at the turn-on voltage which is more significant since it determines the bandgap of the GaInNAs QW.

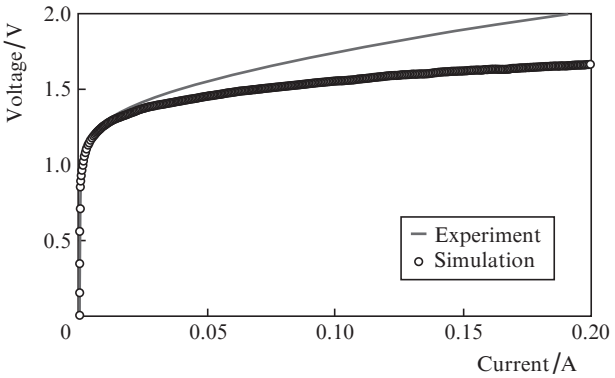

Figure 9. Voltage–current characteristics of the GaInNAs laser diode.

Figure 10 shows the output spectrum characteristic for the simulated and fabricated GaInNAs laser diode. The lasing wavelength obtained for the fabricated device is around 1.261 μm while the simulated device emission wavelength is around 1.293 μm. The blue-shifting of the fabricated device emission wavelength is due to the post-growth annealing treatment of the actual sample during crystal growth and device fabrication. The spectrum blue-shifting induced by thermal annealing is primarily attributed by the rearrangement of local nitrogen bonding configurations and the interdiffusions between gallium and indium atoms across the GaInNAs QW interfaces [14]. A longer emission wavelength is demonstrated

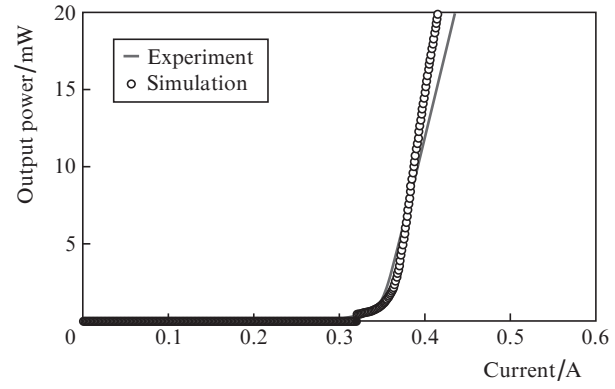

Figure 8. Light–current characteristics of the GaInNAs laser diode.

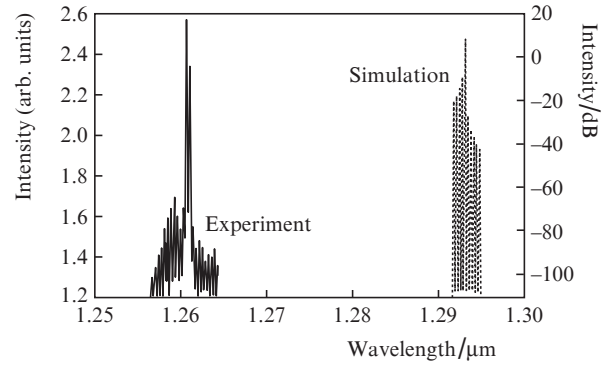

Figure 10. Output spectra of the GaInNAs laser diode.

by the simulated device because the device model is based on a perfectly grown GaInNAs laser diode which does not include the crystal growth drawbacks mentioned above.

4. Conclusions

We have presented a comprehensive study of theoretical optical properties of the GaInNAs laser diode for the long-wavelength semiconductor laser operation. The optimised PL spectrum based on the GaNAs bowing parameter fitting and consideration of the many-body effect theory has shown a high degree of agreement between theoretical and experimental results for the GaInNAs laser diode. This fact creates a beneficial platform for further GaInNAs device design and study since the theoretical physics of the GaInNAs material is still at the initial stage of development.

Acknowledgements. The authors thank Telekom Malaysia for the research funding and CHREA-CNRS for the epiwafer scientific collaboration.

References

1. Wei J., Xia F., Li C., Forrest S.R. *IEEE Photon. Technol. Lett*., **14**, 597 (2002).
2. Zhang Y.G., Chen J.X., Chen Y.Q., Qi M., Li A.Z., Frojdh K., Stoltz B. *J. Crystal Growth*., **227**, 329 (2001).
3. Bank S.R., Bae H., Goddard L.L., Yuen H.B., Wistey M.A., Kudrawiec R., Harris J.S. Jr. *IEEE J. Quantum Electron*., **43**, 773 (2007).
4. Hetterich M., Dawson M.D., Egorov A.Y., Bernklau D., Riechert H. *Appl. Phys. Lett*., **76**, 1030 (2000).
5. Qu Y., Liu C.Y., Yuan S. *Appl. Phys. Lett*., **85**, 5149 (2004).
6. Sarzala R.P., Nakwaski W. *IEE Proc. Optoelectron*., **151**, 417 (2004).
7. Sarzala R.P. *Semicond. Sci. Technol*., **22**, 113 (2007).
8. Chow W.W., Koch S.W., Sargent M. *Semiconductor-Laser Physics* (Berlin: Springer, 1994).
9. Haug H., Koch S.W. *Phys. Rev. A*, **4**, 1887 (1989).
10. Suo Y.K., Yen S.H., Yao M.W., Chen M.L., Liou B.T. *Opt. Commun.*, **275**, 156 (2007).
11. Vurgaftman I., Meyer J.R., Mohan L.R.R. *J. Appl. Phys*., **89**, 5815 (2001).
12. Kimura A., Paulson C.A., Tang H.F., Kuech T.F. *Appl. Phys. Lett*., **84**, 1489 (2004).
13. Yilmaz M., Sun Y., Balkan N., Ulug B., Ulug A., Sopanen M., Reentila O., Mattila M., Fontaine C., Arnoult A. *Microelectr. J*., **40**, 406 (2009).
14. Liu H.F., Xiang N., Zhou H.L., Chua S.J., Yang P., Moser H.O. *J. Crystal Growth*, **301**–**302**, 548 (2007).